

Communication

Nitrogen Dioxide Sensing Using Multilayer Structure of Reduced Graphene Oxide and α -Fe₂O₃

Tadeusz Pisarkiewicz¹, Wojciech Maziarz¹, Artur Małolepszy² , Leszek Stobiński², Dagmara Agnieszka Michoń¹, Aleksandra Szkudlarek³, Marcin Pisarek⁴, Jarosław Kanak¹ and Artur Rydosz^{1,*} 

¹ Institute of Electronics, AGH University of Science and Technology, Al. Mickiewicza 30, 30-059 Kraków, Poland; pisar@agh.edu.pl (T.P.); maziarz@agh.edu.pl (W.M.); dagmaramichon@agh.edu.pl (D.A.M.); kanak@ichf.edu.pl (J.K.)

² Faculty of Chemical and Process Engineering, Warsaw University of Technology, Waryńskiego 1, 00-645 Warsaw, Poland; artur.malolepszy@pw.edu.pl (A.M.); lstob50@hotmail.com (L.S.)

³ Academic Centre for Materials and Nanotechnology, AGH University of Science and Technology, Al. Mickiewicza 30, 30-059 Kraków, Poland; aleszku@agh.edu.pl

⁴ Institute of Physical Chemistry, Polish Academy of Sciences, Kasprzaka 44/52, 01-224 Warsaw, Poland; mpisarek@agh.edu.pl

* Correspondence: rydosz@agh.edu.pl

Abstract: Multilayers consisting of graphene oxide (GO) and α -Fe₂O₃ thin layers were deposited on the ceramic substrates by the spray LbL (layer by layer) coating technique. Graphene oxide was prepared from graphite using the modified Hummers method. Obtained GO flakes reached up to 6 nanometers in thickness and 10 micrometers in lateral size. Iron oxide Fe₂O₃ was obtained by the wet chemical method from FeCl₃ and NH₄OH solution. Manufactured samples were deposited as 3 LbL (GO and Fe₂O₃ layers deposited sequentially) and 6 LbL structures with GO as a bottom layer. Electrical measurements show the decrease of multilayer resistance after the introduction of the oxidizing NO₂ gas to the ambient air atmosphere. The concentration of NO₂ was changed from 1 ppm to 20 ppm. The samples changed their resistance even at temperatures close to room temperature, however, the sensitivity increased with temperature. Fe₂O₃ is known as an n-type semiconductor, but the rGO/Fe₂O₃ hybrid structure behaved similarly to rGO, which is p-type. Both chemisorbed O₂ and NO₂ act as electron traps decreasing the concentration of electrons and increasing the effective multilayer conductivity. An explanation of the observed variations of multilayer structure resistance also the possibility of heterojunctions formation was taken into account.

Keywords: graphen oxide; reduced graphene oxide; α -Fe₂O₃/rGO multilayer; NO₂ sensing



Citation: Pisarkiewicz, T.; Maziarz, W.; Małolepszy, A.; Stobiński, L.; Michoń, D.A.; Szkudlarek, A.; Pisarek, M.; Kanak, J.; Rydosz, A. Nitrogen Dioxide Sensing Using Multilayer Structure of Reduced Graphene Oxide and α -Fe₂O₃. *Sensors* **2021**, *21*, 1011. <https://doi.org/10.3390/s21031011>

Academic Editors: Vittorio M. N. Passaro

Received: 11 December 2020

Accepted: 1 February 2021

Published: 2 February 2021

Publisher's Note: MDPI stays neutral with regard to jurisdictional claims in published maps and institutional affiliations.



Copyright: © 2021 by the authors. Licensee MDPI, Basel, Switzerland. This article is an open access article distributed under the terms and conditions of the Creative Commons Attribution (CC BY) license (<https://creativecommons.org/licenses/by/4.0/>).

1. Introduction

Nitrogen dioxide is a typical air pollutant, being a component of motor vehicle exhaust gas and is also generated in the house and industrial combustion processes. High-temperature combustion leads to an increase in NO_x emissions. The early applications of NO_x detectors for diesel engine exhausts utilized dense zirconia-based electrolytes. It is shown in more recent investigations of nitrogen oxide sensors that good results can be obtained by integrating the sensor with NO_x trap materials [1] or by the use of LaSrMnO₃ type perovskite electrodes [2]. However, the sensors connected with vehicles exhaust work at elevated temperatures, frequently exceeding 300 °C. Exposures to NO₂ are also dangerous for the respiratory system; the presence of nitrogen dioxide in the atmosphere is a cause of photochemical smog and acid rains. Manufacturing of inexpensive NO₂ sensors working at low temperatures is therefore of high importance.

One of the materials recently investigated in gas sensors technology is graphene and structures based on graphene. There are many attempts to increase the sensitivity of graphene-based sensors in view of interaction with the ambient gas atmosphere, enabling practical applications. Pure monolayer graphene with a large surface area and

a high conductivity is a good candidate for high-performance gas sensors. However, its production methods as epitaxial growth or chemical vapor deposition, are known as cost-prohibitive with small-scale yield. Modified graphene materials, i.e., graphene oxide (GO) or its reduced form (rGO), can be much easier manufactured, and their specific properties caused by lattice defects connected with, e.g., oxygen functional groups enhance absorption of ambient gas molecules. Increased sensitivity of rGO can be obtained by hybridization of this material with typical in gas sensor technology metal oxides (MOX), as SnO₂ [3–5], WO₃ [6,7], TiO₂ [8,9], In₂O₃ [10], and ZnO [11,12]. One observes also hybridization of rGO with metal disulfides, as MoS₂ [13–15] and WS₂ [16], conducting polymers (graphene/PANI [17]) or with metal nanoparticles like Cu [18], Pt [19], Pd [20], and Pd-Pt [21]. It was also discovered that the working temperature of graphene/metal oxide sensors was lower than that of MOX sensors and sometimes can even reach room temperature (RT) [22–25]. Good sensitivity of GO to acetone at room temperature was obtained recently by using a microwave-based gas sensor realized as a coupled-line section covered with a graphene oxide film [26].

Another gas-sensitive oxide, α -Fe₂O₃ (hematite), is recently investigated as a NO₂ sensor [27] but more frequently in the form of a nanocomposite with rGO [28–30]. The nanocomposites of α -Fe₂O₃/rGO are also used in detection of acetone [31,32], ethanol [33,34], and ethylene [35]. Among all crystal phases of iron oxide, essentially α -Fe₂O₃ is used in gas sensors technology. This phase is the most stable, environmentally friendly, sensitive, and easy in preparation. Mesoporous α -Fe₂O₃ samples with a large specific surface area were obtained with the use of templates [36,37]. Comparison of sensitivities for α -Fe₂O₃ and γ -Fe₂O₃ phases and their mixture is analyzed in [38].

Sensors of NO₂ based on hematite, as can be inferred from the literature (e.g., see discussion in [27]), work at rather elevated temperatures of order 200 °C. In comparison to pure hematite, improved sensing properties vs. NO₂ were obtained in hybrid nanocomposites rGO/Fe₂O₃ obtained by a facile hydrothermal method [28]. The enhanced response of the nanocomposite at RT was 3.86, compared to 1.38 for pure rGO. In [29] graphene-encapsulated α -Fe₂O₃ hybrids were investigated. The samples revealed good NO₂ sensing properties at RT with the response time of order a few minutes. In this case, the hybrid was obtained by the hydrolysis of Fe³⁺ ions in the colloidal solution of GO and following hydrothermal procedure. The hydrothermal synthesis at 120 °C was applied by the authors of [30] to manufacture α

α -Fe₂O₃/rGO nanocomposites. In effect, nanosphere-like α -Fe₂O₃ of 40–50 nm diameters and single intercalated sheets of rGO were obtained.

In the present work, α -Fe₂O₃ and rGO were obtained separately and deposited on the substrate in the form of a multilayer by the spray method. Such a deposition method allowed for easy formation of slits and pores between the GO sheets, making diffusion of the ambient gas easier. Good sensitivity to NO₂ was also obtained at temperatures close to RT but with quite high response and recovery times.

2. Materials and Methods

2.1. Sample Preparation

Graphene oxide (GO) was prepared using a wet chemical method from graphite (modified Hummers method). Obtained flakes consisted of 6–7 graphene layers with a total thickness of ca. 6 nm and reached the lateral size up to a few micrometers (manufacturing procedure of GO and rGO is described in detail in [39]). Ferric oxide α -Fe₂O₃ was also obtained by the wet chemical method as follows: to 100 mL of 0.1 M FeCl₃, 300 mL of 0.1 M NH₄OH solution was added. An obtained reddish brown suspension was heated for 60 min at 100 °C. The precipitate was washed with warm water on a filter with pore size of 0.2 μ m. Both GO and Fe₂O₃ were deposited on the substrate by spraying, as is schematically illustrated in Figure 1.

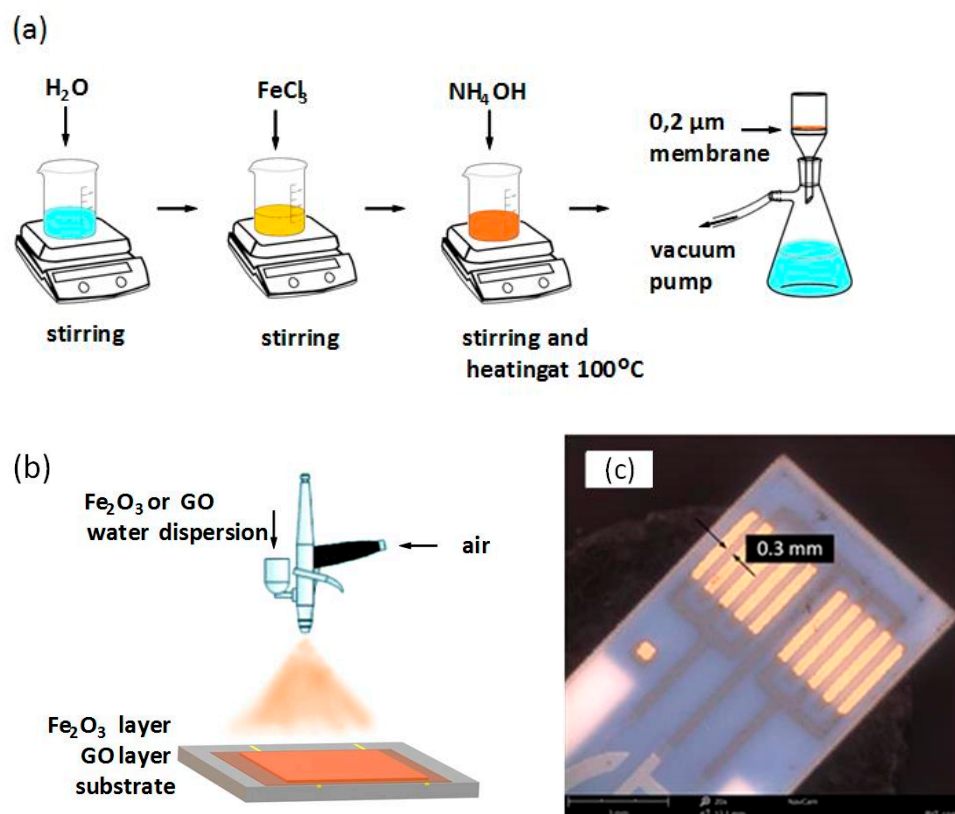


Figure 1. (a) Illustration of the manufacturing process of α - Fe_2O_3 , (b) preparation of GO/ α - Fe_2O_3 multilayer by the spraying method, and (c) outlook of the ceramic substrate used for deposition of the multilayer for electrical measurements.

The GO/ Fe_2O_3 multilayer structure was deposited by LbL (layer by layer) coating technique using alumina substrate with interdigitated Au electrodes manufactured in thick film technology. Separation between electrodes was 0.3 mm. The geometry of electrodes with adequate masking enabled the deposition of two different structures with, e.g., different thicknesses. For investigations, two kinds of samples were prepared: 3 LbL structure consisting of 3 layers (Fe_2O_3 -GO- Fe_2O_3) and 6 LbL structure (3 Fe_2O_3 and 3 GO layers) with Fe_2O_3 layer always on top.

2.2. Electrical Measurements

Measurements of sensor resistance were performed in conditions of selected temperature, humidity, and ambient atmosphere composition. The high-quality equipment (electrometer, current and voltage sources, scanners, mass flow controllers) of Agilent (Agilent Technologies, Santa Clara, CA, USA), Keithley (Keithley Instruments Inc., Cleveland, OH, USA) and MKS (MKS Instruments, Andover, MA, USA) manufacturers was used. The measurement chamber contained the sample, Pt 100 temperature probe and digital humidity sensor. The current was measured by an electrometer working in a constant voltage mode. Measurements of resistance varying in a range over nine orders of magnitude were possible. The temperature inside the chamber was changed by applying the voltage from an additional power source. All devices were controlled from the LabView custom application of Agilent Technologies interface card. The required NO_2 gas concentration was obtained by controlling the ratio of gas to airflow rates. The humidity of the gas atmosphere was always kept constant with $\text{RH} = 50\%$ (detailed description of the measurement setup is given in [40]).

3. Results and Discussion

3.1. Structural and Morphological Characteristics

TEM measurements were performed with the help of high resolution scanning electron microscope HITACHI S-5500 (HITACHI Ltd., Tokyo, Japan) in a transmission mode. An example of a TEM image for the GO sample is shown in Figure 2a. Different transparencies for attenuated electron beams were caused by the stacking nanostructure of the investigated layers. Dark areas indicate the overlap of several layers. SEM pictures were obtained with the help of FEI Versa 3D Dual Beam microscope (Thermo Fisher Scientific, Waltham, MA, USA). In Figure 2b, one can see the flakes of GO sample deposited on Si/SiO₂ substrate.

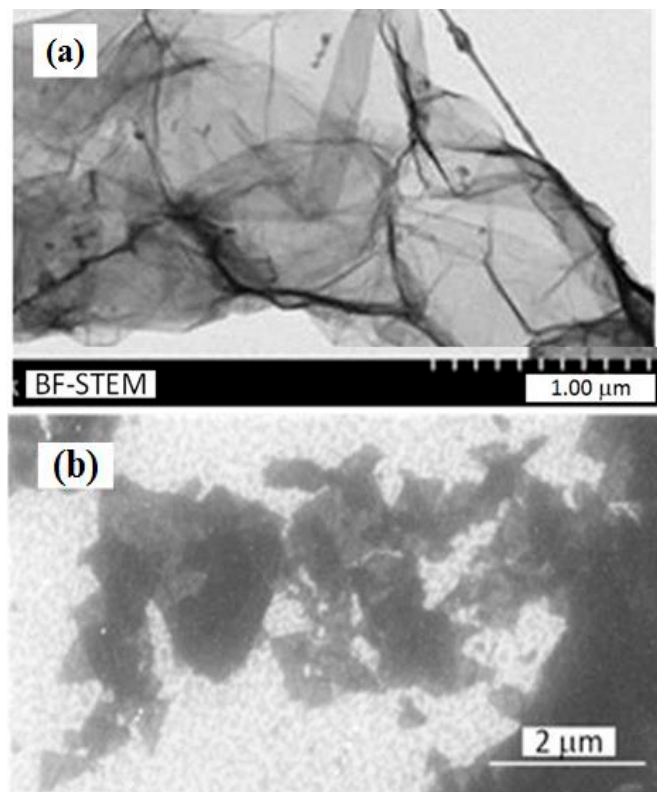


Figure 2. (a) TEM and (b) SEM image of GO flakes.

In the image of GO/Fe₂O₃ nanostructure, Figure 3a, one can see both gray areas of GO flakes and white spots of Fe₂O₃ nanoparticles of average dimension ca 100 nm, covering GO flakes. The XRD patterns, Figure 3b, were obtained by using an XRD diffractometer Bruker AXS D8 Advance Cr (K α 2.2910 Å) (Bruker AXS GmbH, Karlsruhe, Germany) with vanadium filter 0.015 mm. Observed peaks belong to the crystal planes of the hematite phase, which can be indexed to the rhombohedral structure of α -Fe₂O₃ and their positions are in accordance with JCPDS 86-0550 card. Analysis of the X-ray reflectivity for GO/Fe₂O₃ nanostructure enabled the determination of its thickness, equal 47.5 nm, and the RMS of surface roughness, 1.42 nm.

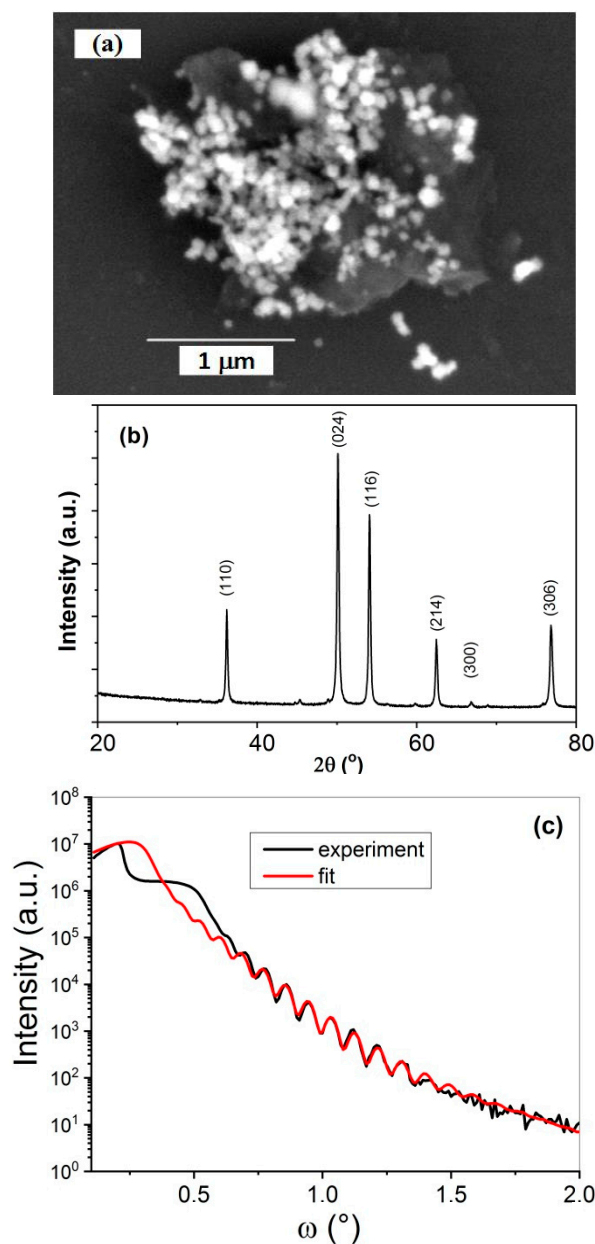


Figure 3. (a) SEM image of GO/ α -Fe₂O₃ structure, (b) X-ray diffraction pattern for α -Fe₂O₃, (c) X-ray reflectivity pattern for GO/ α -Fe₂O₃.

3.2. Chemical Composition

The surface chemistry of investigated samples was analyzed using X-ray photoelectron spectroscopy. A Microlab 350 (Thermo Electron, VG Scientific) spectrometer with non-monochromatic Al K α radiation ($h\nu = 1486.6$ eV, power 300 W, voltage 15 kV) was used for this purpose. The analyzed area was 2×5 mm. The hemispherical analyzer was used for collecting the high-resolution (HR) XPS spectra with the following parameters: pass energy 40 eV, energy step size 0.1 eV. The collected XPS spectra were fitted using the Avantage software (version 5.9911, Thermo Fisher Scientific), where a Smart function of background subtraction was used to obtain XPS signal intensity and an asymmetric Gaussian/Lorentzian mixed-function was applied. The position of the carbon C1s peak was assumed to be at 284.4 eV and used as an internal standard to determine the binding energy of other photoelectron peaks. XPS spectra for GO/Fe₂O₃ structure are shown in Figure 4 and for rGO/Fe₂O₃ structure in Figure 5.

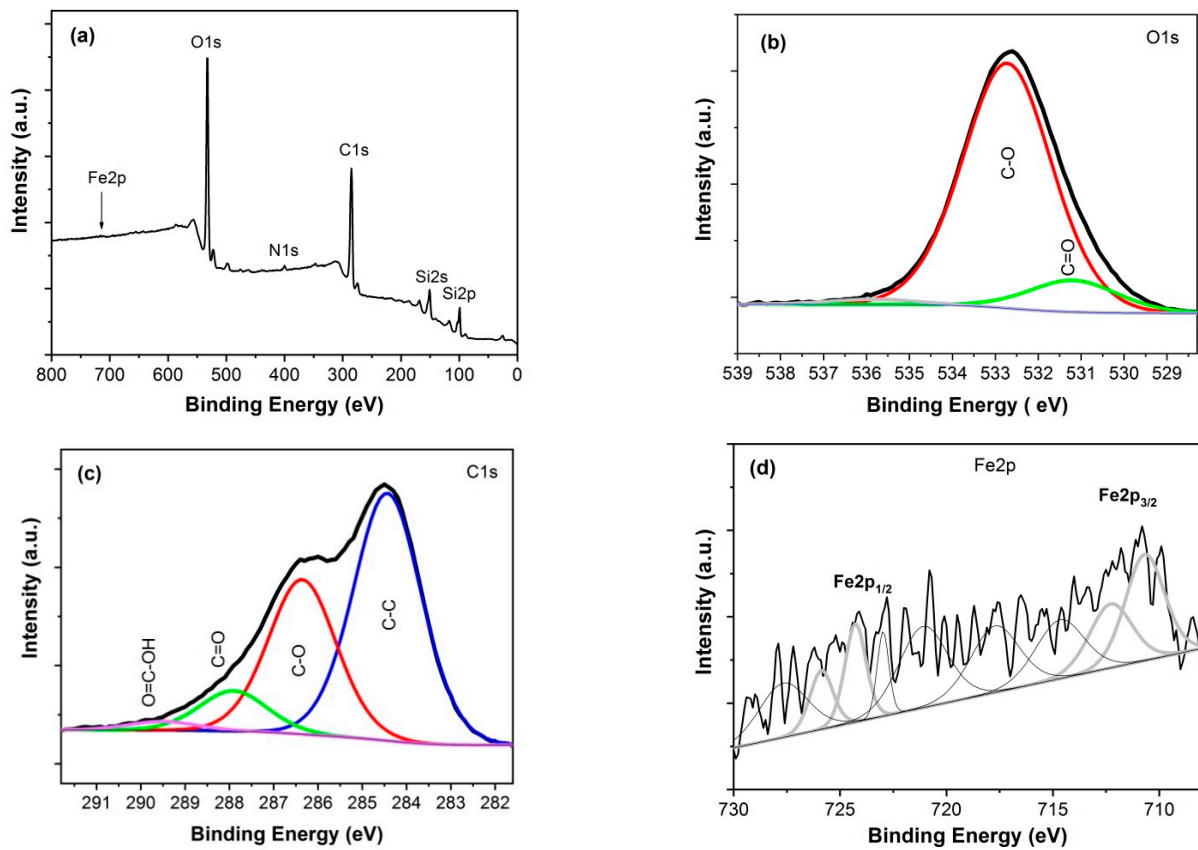


Figure 4. XPS spectra for GO/Fe₂O₃ multilayer: (a) wide scan, (b) HR O1s, (c) HR C1s, (d) HR Fe2p.

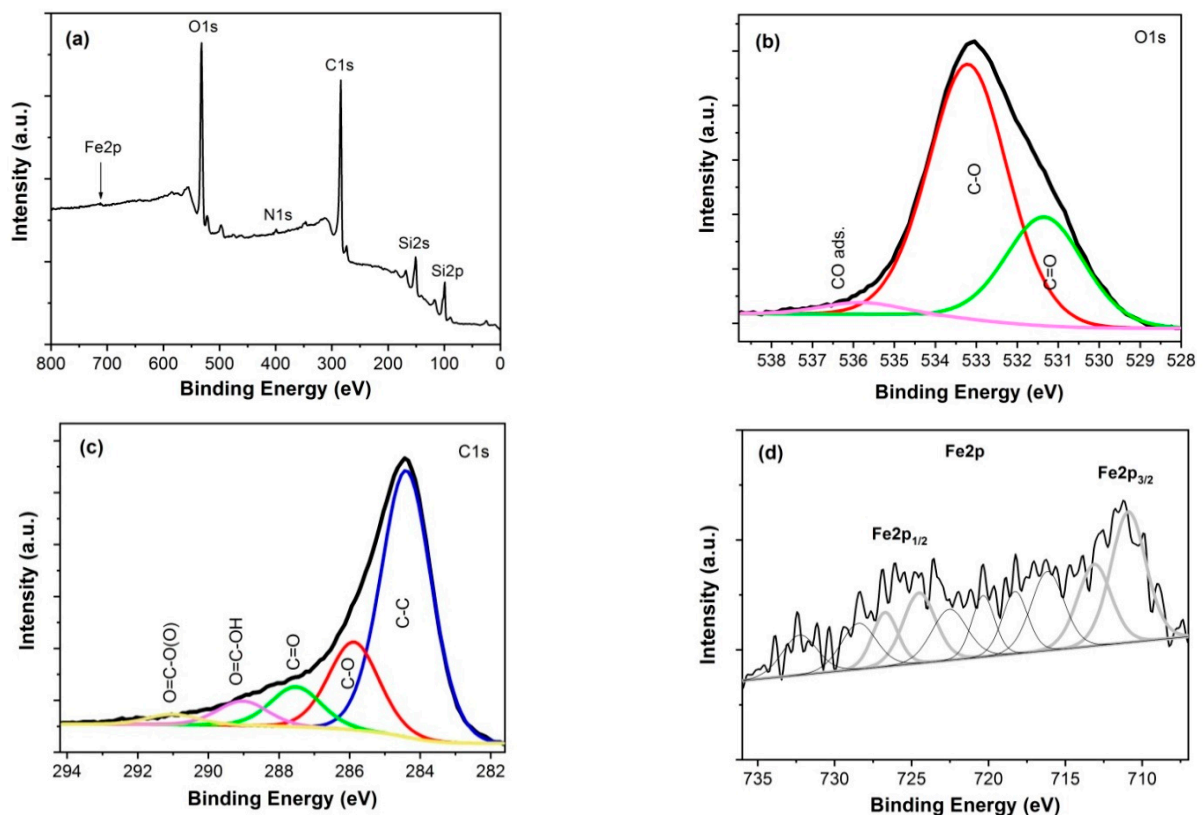


Figure 5. XPS spectra for rGO/Fe₂O₃ multilayer: (a) wide scan, (b) HR O1s, (c) HR C1s, (d) HR Fe2p.

A significant decrease of oxygen content in the samples after reduction is seen from the comparison of Figures 4 and 5. The percent concentrations of oxygen-containing bonds C-O and C=O in both kinds of samples are collected in Table 1. In particular, the decrease in C-O bonds is clearly seen after thermal reduction (decrease from 34.2% to 20.5%). Similar observations are reported by other investigators of rGO/ α -Fe₂O₃ composites, [28,32].

Table 1. The percent contents of C1s chemical bonds in GO/Fe₂O₃ and rGO/Fe₂O₃ samples. The results are normalized to 100% for the C1s peak.

Sample	Chemical Bonds				
GO/Fe ₂ O ₃	C-C (284.4 eV)	C-O (286.4 eV)	C=O (287.9 eV)	O=C-OH (289.5 eV)	-
	54.9%	34.2%	8.9%	2.0%	-
rGO/Fe ₂ O ₃	C-C (284.4 eV)	C-O (285.9 eV)	C=O (287.5 eV)	O=C-OH (289.0 eV)	O=C-O(O) (291.0 eV)
	62.2%	20.5%	9.3%	5.6%	2.4%

The recorded XR-XPS spectra of Fe2p revealed the chemical state of iron. Two wide peaks for both structures, located at the binding energies of ca. 711.0 eV and ca. 725.0 eV for Fe2p_{3/2} and Fe2p_{1/2}, respectively, are characteristic for Fe³⁺ species in α -Fe₂O₃, which is in good agreement with other reports, e.g., [29,31].

3.3. Gas Sensing Properties

Measurements of resistance for GO/Fe₂O₃ multilayers in response to oxidizing NO₂ atmosphere indicate that the structures behave as p-type semiconductors (under oxidizing atmosphere resistance of the sample decreases). Calculated gas response defined as $S = (R_a - R_g)/R_a$ where R_a and R_g are the sensor resistances in air and NO₂, respectively, indicate that the structures are sensitive even at temperatures as low as 30 °C (Figure 6a,b). With increasing working temperature, the response also increased, as is shown for the structure GO/Fe₂O₃ 6 LbL with an increased number of layers, Figure 6c. As can be noticed, an increase in the number of layers in the structure does not influence the response remarkably. Variation of the baseline resistance with time at a constant NO₂ concentration is shown in Figure 6d, and the comparison of sensitivities for the 6LbL multilayer and the single rGO layer is shown in Figure 6e.

The selectivity of GO/Fe₂O₃ 6LbL structure was tested by exposing the sensor to different interference gases, both oxidizing and reducing, as shown in Figure 7. Comparing the response to acetone (1.2% at 25 ppm) and hydrogen (0.9% at 50 ppm) with that to NO₂, one can summarize that the influence of the tested interference gases is negligible. However, the influence of humidity on the sensor response is remarkable and is clearly seen at elevated temperatures. The example measurements of that response at 90 °C in a wide range of RH is shown in Figure 7b. The results indicate that both the increase and decrease of RH in comparison to 50% give variations of the response not higher than $\pm 5\%$.

The response and recovery times of the structures are high, especially in the low operation temperature range. With increasing working temperature, these times significantly decreased, as shown in Figure 8 and Table 2.

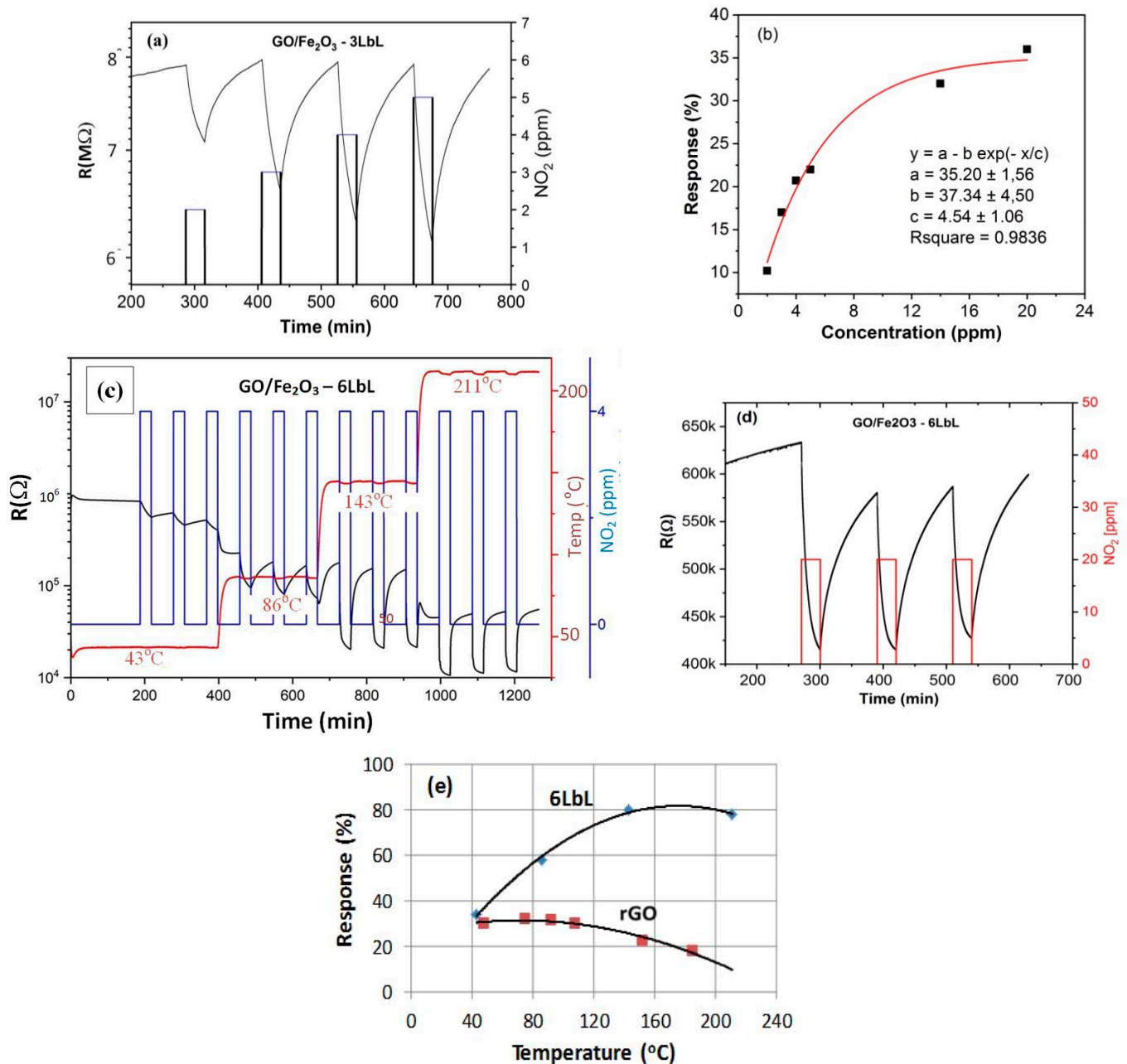


Figure 6. (a) Variation of resistance with time for GO/Fe₂O₃ 3LbL structure with increasing NO₂ concentration at the temperature of 30 °C with a calculated response of this structure for increasing NO₂ concentration (b); (c) variation of resistance for GO/Fe₂O₃ 6 LbL structure with changing sensor temperature at 4 ppm NO₂ and (d) at 20 ppm NO₂ at a constant temperature 30 °C; (e) comparison of responses for samples GO/Fe₂O₃ 6 LbL and single rGO layer with increasing measurement temperature at 4 ppm NO₂.

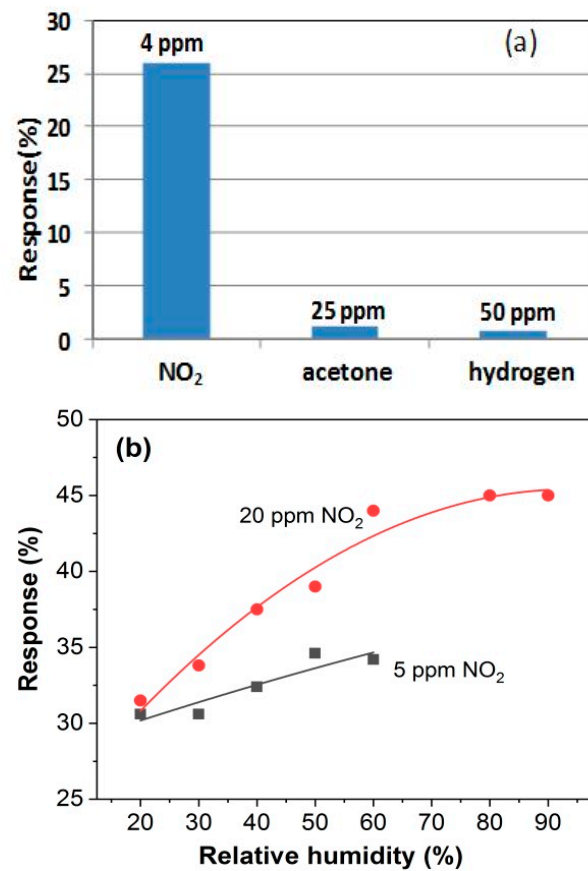


Figure 7. (a) The response of GO/Fe₂O₃ 6LbL structure to different gases at room temperature and (b) variation of this response with the change of relative humidity at 90 °C.

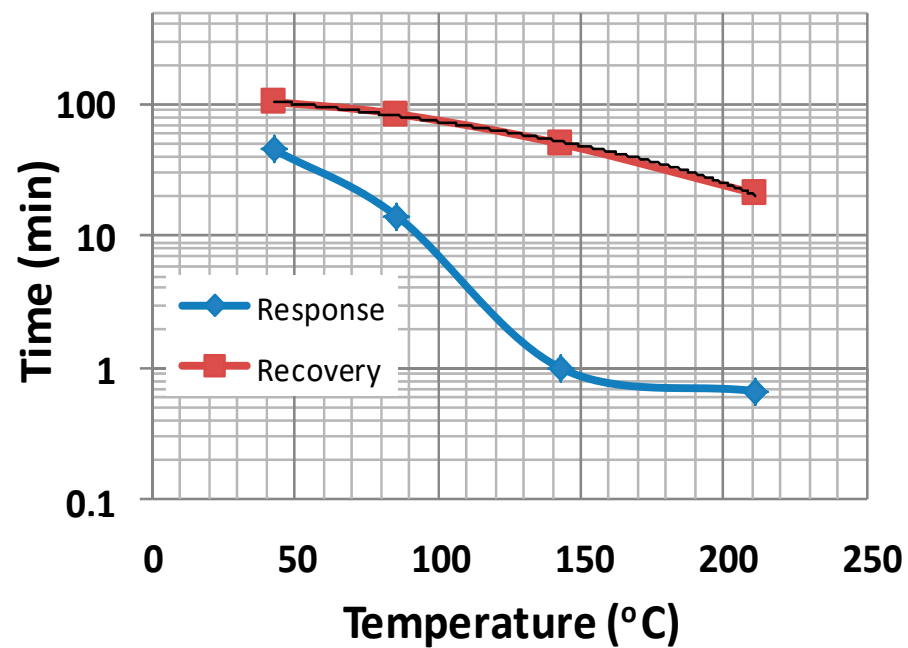


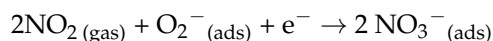
Figure 8. Response and recovery times vs. temperature for the sample shown in Figure 6c.

Table 2. Variation of response and recovery times with temperature for sample GO/Fe₂O₃ 6 LbL.

Temperature (°C)	Response Time t_{res} (min)	Recovery Time t_{rec} (min)	t_{rec}/t_{res}
43	45	104	2.31
86	14	84	6
143	1	50	50
211	0.67	21	31.3

3.4. Gas Sensing Mechanism

Fe₂O₃ is known as an n-type semiconductor, but the rGO/Fe₂O₃ hybrid structure behaves similarly to p-type rGO. Both chemisorbed O₂ and NO₂ act as electron traps decreasing the concentration of electrons. This is clearly seen in rGO in the decrease of resistance (hole density increases). Pure Fe₂O₃ is nearly insensitive to NO₂, but in rGO/Fe₂O₃ composition, NO₂ reacts with O₂[−] adsorbed on Fe₂O₃ surface, forming an intermediate NO₃[−] complex what was suggested in [30]



As a result, the unbalance of charge on the surface of Fe₂O₃ is compensated by transferring additional electrons from rGO to Fe₂O₃ surface, which results in additional holes in rGO, Figure 9, and then the increase in conductivity.

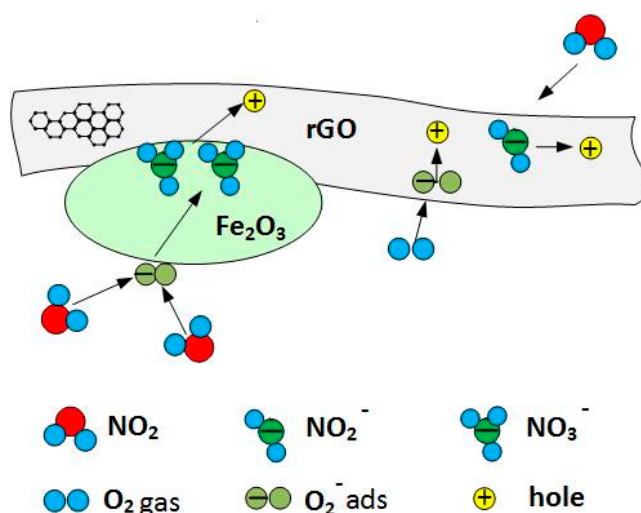


Figure 9. Interaction of NO₂ gas with oxygen adsorbed on Fe₂O₃ surface can effectively increase the concentration of holes in rGO.

In Table 2, O₃ on the increased sensitivity to NO₂ can be understood from Figure 10. At the interface between rGO flakes and Fe₂O₃ grains, the p-n heterojunctions can be formed. The numerical value of work function for rGO was taken from [41], and the energy gap was evaluated from [42] for oxygen content in rGO equal O/C = 10%, as previously determined in elemental composition experiments [40]. The work function for Fe₂O₃ was taken from Guo et al. [31]. The difference in work functions of both materials causes the transfer of electrons from rGO to Fe₂O₃ and holes in the opposite direction. In effect, the hole accumulation region is formed on the p-rGO side. The concentration of holes in the accumulation layer on the p-side increases additionally after interaction with NO₂, leading to the increased conductivity of GO flakes in the presence of NO₂ gas, as schematically shown in Figure 11.

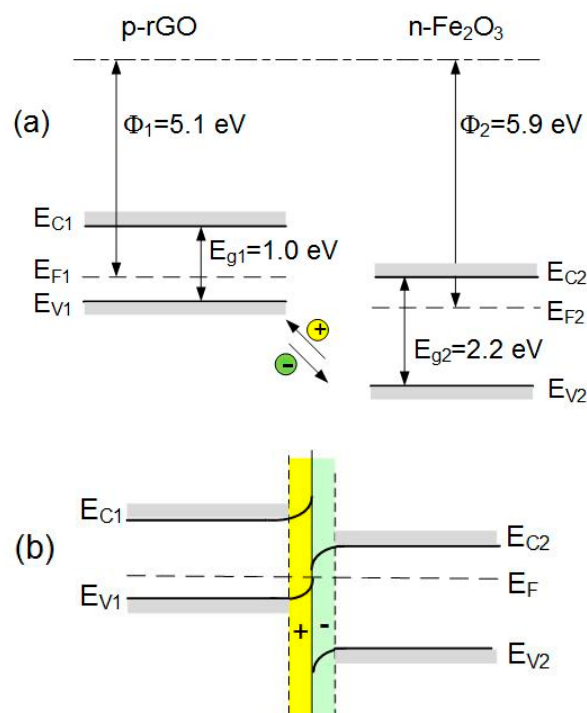


Figure 10. Diagram of energy bands of p-rGO and n-Fe₂O₃ before (a) and after (b) contact with the formation of a p-n heterojunction.

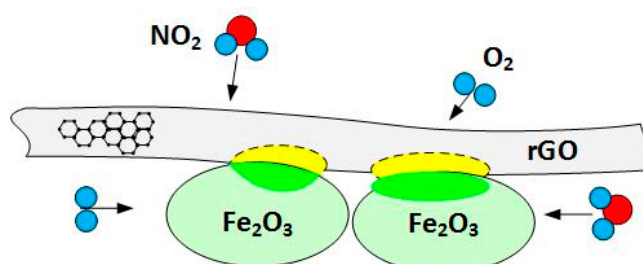


Figure 11. Interaction of Fe₂O₃ grains with rGO flakes leading to the formation of hole accumulation regions in rGO flakes.

Potential barriers between Fe₂O₃ grains were not taken into account as the multilayer structure in response to NO₂ behaves as a p-type semiconductor, then rGO layers play the essential role in conductivity.

As it was mentioned, the spray deposition technology allowed for easy formation of slits between the GO sheets, and additionally, Fe₂O₃ prevented these sheets from restacking. The slits can act as channels for gas diffusion, providing a higher number of active sites for the interaction with nitrogen dioxide, thus influencing the electrical transport.

4. Conclusions

Among air pollutants, NO₂ is one of the most harmful gases, and measurements of its concentration with the help of inexpensive chemoresistive structures with very small power consumption are of great importance. In contrary to the pure Fe₂O₃ with small sensitivity to NO₂ in the low-temperature range, rGO/Fe₂O₃ multilayer structures indicated good sensitivity to low concentrations of NO₂ in the ambient air, going down to 1 ppm. Both materials of the structure were easily obtained by the wet chemical method and were sprayed on the substrate to form the needed composition. The sensitivity of the multilayer increased with temperature. Response time of order 1 min was possible to obtain at temperatures below 150 °C, but the recovery time was still high, of order tens

of minutes. An increase in the number of layers of the structure did not influence the response remarkably. The sensing behavior of the multilayer structure was explained by both individual interactions of constituting materials with the ambient oxidizing gas and by the formation of heterojunctions at the contact regions of GO and Fe₂O₃.

Author Contributions: Conceptualization and methodology, T.P., L.S., and A.R.; writing original draft, T.P.; measurements, W.M., A.S.; M.P., and J.K., sample preparation, A.M.; review and editing, A.R., D.A.M., and A.M. All authors have read and agreed to the published version of the manuscript.

Funding: This research received no external funding.

Institutional Review Board Statement: Not applicable.

Informed Consent Statement: Not applicable.

Data Availability Statement: Data Availability on request.

Acknowledgments: This work was supported by the National Science Centre, Poland NCN UMO-2016/23/B/ST7/00894 and National Science Centre, NCN Poland 2017/26/D/ST7/00355.

Conflicts of Interest: The authors declare no conflict of interest.

References

1. Geupel, A.; Schönauer, D.; Röder-Roith, U.; Kubinski, D.J.; Mulla, S.; Ballinger, T.H.; Chen, H.-Y.; Visser, J.H.; Moos, R. Integrating nitrogen oxide sensor: A novel concept for measuring low concentrations in the exhaust gas. *Sens. Actuators B Chem.* **2010**, *145*, 756–761. [[CrossRef](#)]
2. Pal, N.; Murray, E. Dense LaSrMnO₃ composite electrodes for NO_x sensing. *Sens. Actuators B Chem.* **2018**, *256*, 351–358. [[CrossRef](#)]
3. Liu, S.; Wang, Z.Y.; Zhang, Y.; Li, J.C.; Zhang, T. Sulfonated graphene anchored with tin oxide nanoparticles for detection of nitrogen dioxide at room temperature with enhanced sensitivity performances. *Sens. Actuators B Chem.* **2016**, *228*, 134–143. [[CrossRef](#)]
4. Feng, Q.; Li, X.; Wang, J. Percolation effect of reduced graphene oxide (rGO) on ammonia sensing of rGO-SnO₂ composite based sensor. *Sens. Actuators B Chem.* **2017**, *243*, 1115–1126. [[CrossRef](#)]
5. Xiao, Y.; Yang, Q.; Wang, Z.; Zhang, R.; Gao, Y.; Sun, P.; Sun, Y.; Lu, G. Improvement of NO₂ gas sensing performance based on discoid tin oxide modified by reduced graphene oxide. *Sens. Actuators B Chem.* **2016**, *227*, 419–426. [[CrossRef](#)]
6. Punetha, D.; Kumar Pandey, S. Sensitivity Enhancement of Ammonia Gas Sensor Based on Hydrothermally Synthesized rGO/WO₃ Nanocomposites. *IEEE Sens. J.* **2020**, *20*, 1738–1745. [[CrossRef](#)]
7. Srivastava, S.; Jain, K.; Singh, V.N.; Singh, S.; Vijayan, N.; Dilawar, N.; Gupta, G.; Senguttuvan, T.D. Faster response of NO₂ sensing in graphene-WO₃ nanocomposites. *Nanotechnology* **2012**, *23*, 205501. [[CrossRef](#)]
8. Galstyan, V.; Ponzoni, A.; Kholmanov, I.; Natile, M.M.; Comini, E.; Nematov, S.; Sberveglieri, G. Reduced Graphene Oxide-TiO₂ Nanotube Composite: Comprehensive Study for Gas-Sensing Applications. *ACS Appl. Nano Mater.* **2018**, *1*, 7098–7105. [[CrossRef](#)]
9. Lin, W.-D.; Liao, C.-T.; Chang, T.-C.; Chen, S.-H.; Wu, R.-J. Humidity sensing properties of novel graphene/TiO₂ composites by sol-gel process. *Sens. Actuators B Chem.* **2015**, *209*, 555–561. [[CrossRef](#)]
10. Gu, F.; Nie, R.; Han, D.; Wang, Z. In₂O₃-graphene nanocomposite based gas sensor for selective detection of NO₂ at room temperature. *Sens. Actuators B Chem.* **2015**, *219*, 94–99. [[CrossRef](#)]
11. Liu, S.; Yu, B.; Zhang, H.; Fei, T.; Zhang, T. Enhancing NO₂ gas sensing performances at room temperature based on reduced graphene oxide-ZnO nanoparticles hybrids. *Sens. Actuators B Chem.* **2014**, *202*, 272–278. [[CrossRef](#)]
12. Ugale, A.D.; Umarji, G.G.; Jung, S.H.; Deshpande, N.G.; Lee, W.; Cho, H.K.; Yoo, J. ZnO decorated flexible and strong graphene fibers for sensing NO₂ and H₂S at room temperature. *Sens. Actuators B Chem.* **2020**, *308*, 127690. [[CrossRef](#)]
13. Wang, Z.; Zhang, T.; Zhao, C.; Han, T.; Fei, T.; Liu, S.; Lu, G. Rational synthesis of molybdenum disulfide nanoparticles decorated reduced graphene oxide hybrids and their application for high-performance NO₂ sensing. *Sens. Actuators B Chem.* **2018**, *260*, 508–518. [[CrossRef](#)]
14. Zhou, Y.; Liu, G.; Zhu, X.; Guo, Y. Ultrasensitive NO₂ gas-sensing based on rGO/MoS₂ nanocomposite film at low temperature. *Sens. Actuators B Chem.* **2017**, *251*, 280–290. [[CrossRef](#)]
15. Hou, X.; Wang, Z.; Fan, G.; Ji, H.; Yi, S.; Li, T.; Wang, Y.; Zhang, Z.; Yuan, L.; Zhang, R.; et al. Hierarchical three-dimensional MoS₂/GO hybrid nanostructures for trimethylamine-sensing applications with high sensitivity and selectivity. *Sens. Actuators B Chem.* **2020**, *317*, 128236. [[CrossRef](#)]
16. Wang, X.; Gu, D.; Li, X.; Lin, S.; Zhao, S.; Kovalenko, V.V.; Gaskov, A.M. Reduced graphene oxide hybridized with WS₂ nanoflakes based heterojunctions for selective ammonia sensors at room temperature. *Sens. Actuators B Chem.* **2019**, *282*, 290–299. [[CrossRef](#)]
17. Wu, Z.; Chen, X.; Zhu, S.; Zhou, Z.; Yao, Y.; Quan, W.; Liu, B. Room Temperature Methane Sensor Based on Graphene Nanosheets/Polyaniline Nanocomposite Thin Film. *IEEE Sens. J.* **2012**, *13*, 777–782. [[CrossRef](#)]
18. Gil Na, H.; Cho, H.Y.; Kwon, Y.J.; Kang, S.Y.; Lee, C.; Jung, T.K.; Lee, H.-S.; Kim, H.W. Reduced graphene oxide functionalized with Cu nanoparticles: Fabrication, structure, and sensing properties. *Thin Solid Film.* **2015**, *588*, 11–18. [[CrossRef](#)]

19. Shafiei, M.; Spizzirri, P.G.; Arsat, R.; Yu, J.; du Plessis, J.; Dubin, S.; Ianer, R.B.; Kalantar-Zadeh, K.; Wlodarski, W. Platinum/graphene nanosheet/SiC contacts and their application for hydrogen gas sensing. *J. Phys. Chem. C* **2010**, *114*, 13796–13801. [[CrossRef](#)]
20. Cho, B.; Yoon, J.; Hahm, M.G.; Kim, D.-H.; Kim, A.R.; Khang, Y.H.; Park, S.-W.; Lee, Y.-J.; Park, S.-G.; Kwon, J.-D.; et al. Graphene-based gas sensor: Metal decoration effect and application to a flexible device. *J. Mater. Chem. C* **2014**, *2*, 5280–5285.
21. Kumar, R.; Varandani, D.; Mehta, B.R.; Singh, V.N.; Wen, Z.; Feng, X.; Müllen, K. Fast response and recovery of hydrogen sensing in Pd–Pt nanoparticle–graphene composite layers. *Nanotechnology* **2011**, *22*, 275719. [[CrossRef](#)] [[PubMed](#)]
22. Drmosh, Q.A.; Hendi, A.H.; Hossain, M.K.; Yamani, Z.H.; Moqbel, R.A.; Hezam, A.; Gondal, M.A. UV-activated gold decorated rGO/ZnO heterostructured nanocomposite sensor for efficient room temperature H₂ detection. *Sens. Actuators B Chem.* **2019**, *290*, 666–675. [[CrossRef](#)]
23. Guo, W.; Zhou, Q.; Zhang, J.; Fu, M.; Radacsi, N.; Li, Y. Hydrothermal synthesis of Bi-doped SnO₂/rGO nanocomposites and the enhanced gas sensing performance to benzene. *Sens. Actuators B Chem.* **2019**, *299*, 126959. [[CrossRef](#)]
24. Sun, D.; Luo, Y.; Debliquy, M.; Zhang, C. Graphene-enhanced metal oxide gas sensors at room temperature: A review. *Beilstein J. Nanotechnol.* **2018**, *9*, 2832–2844. [[CrossRef](#)] [[PubMed](#)]
25. Zhang, C.; Zhang, S.; Yang, Y.; Yu, H.; Dong, X. Highly sensitive H₂S sensors based on metal-organic framework driven γ -Fe₂O₃ on reduced graphene oxide composites at room temperature. *Sens. Actuators B Chem.* **2020**, *325*, 128804. [[CrossRef](#)]
26. Staszek, K.; Szkudlarek, A.; Kawa, M.; Rydosz, A. Microwave system with sensor utilizing GO-based gas-sensitive layer and its application to acetone detection. *Sens. Actuators B Chem.* **2019**, *297*, 126699. [[CrossRef](#)]
27. Hjiri, M.; Aida, M.S.; Neri, G. NO₂ Sensitive Sensor Based on α -Fe₂O₃ Nanoparticles Synthesized via Hydrothermal Technique. *Sensors* **2019**, *19*, 167. [[CrossRef](#)]
28. Zhang, H.; Yu, L.; Li, Q.; Du, Y.; Ruan, S. Reduced graphene oxide/ α -Fe₂O₃ hybrid nanocomposites for room temperature NO₂ sensing. *Sens. Actuators B Chem.* **2017**, *241*, 109–115. [[CrossRef](#)]
29. Zhang, B.; Liu, G.; Cheng, M.; Gao, Y.; Zhao, L.; Li, S.; Liu, F.; Yan, X.; Zhang, T.; Sun, P.; et al. The preparation of reduced graphene oxide-encapsulated α -Fe₂O₃ hybrid and its outstanding NO₂ gas sensing properties at room temperature. *Sens. Actuators B Chem.* **2018**, *261*, 252–263. [[CrossRef](#)]
30. Dong, Y.-L.; Zhang, X.-F.; Cheng, X.; Xu, Y.-M.; Gao, S.; Zhao, H.; Huo, L.-H. Highly selective NO₂ sensor at room temperature based on nanocomposites of hierarchical nanosphere-like α -Fe₂O₃ and reduced graphene oxide. *RSC Adv.* **2014**, *4*, 57493–57500. [[CrossRef](#)]
31. Song, H.; Xia, L.; Jia, X.; Yang, W. Polyhedral α -Fe₂O₃ crystals@RGO nanocomposites: Synthesis, characterization and application in gas sensing. *J. Alloys Compd.* **2018**, *732*, 191–200. [[CrossRef](#)]
32. Guo, L.; Kou, X.; Ding, M.; Wang, C.; Dong, L.; Zhang, H.; Feng, C.; Sun, Y.; Gao, Y.; Sun, P.; et al. Reduced graphene oxide/ α -Fe₂O₃ composite nanofibers for application in gas sensors. *Sens. Actuators B Chem.* **2017**, *244*, 233–242. [[CrossRef](#)]
33. Liang, S.; Zhu, J.; Wang, C.; Yu, S.; Bi, H.; Liu, X.; Wang, X. Fabrication of α -Fe₂O₃@graphene nanostructures for enhanced gas-sensing property to ethanol. *Appl. Surf. Sci.* **2014**, *292*, 278–284. [[CrossRef](#)]
34. Jia, X.; Lian, D.; Shi, B.; Dai, R.; Li, C.; Wu, X. Facile synthesis of α -Fe₂O₃@graphene oxide nanocomposites for enhanced gas-sensing performance to ethanol. *J. Mater. Sci. Mater. Electron.* **2017**, *28*, 12070–12079. [[CrossRef](#)]
35. Li, B.; Li, M.; Meng, F.; Liu, J. Highly selective ethylene sensors using Pd nanoparticles and rGO modified flower-like hierarchical porous α -Fe₂O₃. *Sens. Actuators B Chem.* **2019**, *290*, 396–405. [[CrossRef](#)]
36. Geng, W.; Ge, S.; He, X.; Zhang, S.; Gu, J.; Lai, X.; Wang, H.; Zhang, Q. Volatile Organic Compound Gas-Sensing Properties of Bimodal Porous α -Fe₂O₃ with Ultrahigh Sensitivity and Fast Response. *ACS Appl. Mater. Interfaces* **2018**, *10*, 13702–13711. [[CrossRef](#)]
37. Sun, G.; Chen, H.; Li, Y.; Ma, G.; Zhang, S.; Jia, T.; Cao, J.; Wang, X.; Bala, H.; Zhang, Z. Synthesis and triethylamine sensing properties of mesoporous α -Fe₂O₃ microrods. *Mater. Lett.* **2016**, *178*, 213–216. [[CrossRef](#)]
38. Wang, M.; Hou, T.; Shen, Z.; Zhao, X.; Ji, H. MOF-derived Fe₂O₃: Phase control and effects of phase composition on gas sensing performance. *Sens. Actuators B Chem.* **2019**, *292*, 171–179. [[CrossRef](#)]
39. Stobinski, L.; Lesiak, B.; Malolepszy, A.; Mazurkiewicz, M.; Mierzwa, B.; Zemek, J.; Jiricek, P.; Bieloshapka, I. Graphene oxide and reduced graphene oxide studied by the XRD, TEM and electron spectroscopy methods. *J. Electron Spectrosc. Relat. Phenom.* **2014**, *195*, 145–154. [[CrossRef](#)]
40. Pisarkiewicz, T.; Maziarz, W.; Malolepszy, A.; Stobiński, L.; Michoń, D.; Rydosz, A. Multilayer Structure of Reduced Graphene Oxide and Copper Oxide as a Gas Sensor. *Coatings* **2020**, *10*, 1015. [[CrossRef](#)]
41. Yang, H.; Li, Y.; Yu, D.; Li, L. Seed/catalyst free growth and self-powered photoresponse of vertically aligned ZnO nanorods on reduced graphene oxide nanosheets. *Cryst. Growth Des.* **2016**, *16*, 4831–4838. [[CrossRef](#)]
42. Huang, H.; Li, Z.; She, J.; Wang, W. Oxygen density dependent band gap of reduced graphene oxide. *J. Appl. Phys.* **2012**, *111*, 054317. [[CrossRef](#)]